Research Article Open Access

Yu Liu, Jin Zhou\*, and Zhi-yong Lin

# Numerical study on the standing morphology of an oblique detonation wave under the influence of an incoming boundary layer

**Abstract:** The influence of an incoming boundary layer to the standing morphology of an oblique detonation wave (ODW) induced by a compression ramp is numerically studied in this paper. The Spalart-Allmaras (SA) turbulence model is used to perform simulation of detonation-boundary-layer interactions. Three different wall conditions are applied to realize control on the boundary-layer separation scales. Accordingly, different standing morphologies of the ODWs are obtained, including smooth ODW (without transverse wave) under no-slip, adiabatic wall condition with large-scale separation, abrupt ODW (with transverse wave) under no-slip, cold wall condition with moderate-scale separation, and bow-shaped detached ODW under slip wall condition without a boundary layer.

**Keywords:** oblique detonation wave; standing; boundary

layer; separation

PACS: 47.40.Rs, 82.40.Fp, 47.40.Ki

DOI 10.1515/phys-2015-0007 Received April 1, 2014; accepted July 28, 2014

#### 1 Introduction

It is well known that a ramp-induced shock wave in a supersonic flow can cause the problem of shock waveboundary layer interactions (SWBLI). Since a boundary layer is susceptible to adverse pressure gradient, sepa-

\*Corresponding Author: Jin Zhou: Science and Technology on Scramjet Laboratory, National University of Defense Technology, College of Aerospace Science and Engineering, National University of Defense Technology, 410073 Changsha, China, E-mail: zj706@vip.sina.com

**Yu Liu, Zhi-yong Lin:** Science and Technology on Scramjet Laboratory, National University of Defense Technology, College of Aerospace Science and Engineering, National University of Defense Technology, 410073 Changsha, China, E-mail: yuesefuliu@sina.com

ration often occurs if the shock wave is strong enough. In past decades, many aspects of the SWBLI have been investigated, including incipient separation problem [1-3], the relationship between the pressure plateau value in the separation region and the incoming flow parameters [4, 5], the scaling laws of the separation length [6], heat transfer study [1, 7] and unsteadiness problems [8, 9]. The SWBLI problems mentioned above are all about inert shock wave, compared to which, there are much less studies on detonation-boundary layer interactions. The effect of boundary layer on the propagating detonation wave is first theoretically modeled by Fay [10]. He suggested that the boundary layer behind the detonation wave causes flow divergence and thus curved detonation front, leading to deficit of detonation velocity. This deficit is especially significant in very confined ducts since the flow divergence is considerable relative to the duct dimensions. However, Fay and other researchers' studies [11-14] are focused on detonation wave in quiescent gas where there is no boundary layer ahead of the detonation wave. Also, for the ODW in the supersonic flow, Li [15] et al. investigated the effect of boundary layer on the wedge surface (again, post-detonation) and it was found that the overall detonation structures are almost the same for viscous and inviscid cases. Considering the incoming boundary-layer effect, Choi [16] et al. investigated the combustion induced by incident shock wave-boundary layer interaction in premixed gas. They identified two combustion regimes, i.e., a steady boundary-layer flame held by the separation bubble at the shock impinging point and an unstable oblique detonation wave that propagates forward. If the flow residence time is sufficiently long to accommodate the complete combustion, the detonative explosion is possible. If not, combustion is restricted as boundary-layer flame or oblique shock-induced combustion. Since Choi's investigation is based on the incident shock wave, there is still no research on ramp-induced ODW-boundary layer interactions so far as we know.

As we know, the oblique detonation wave engine (ODWE) [17] is one of important directions for future de-

16 — Y. Liu et al. DE GRUYTER OPEN

velopment of hypersonic flights. In past decades, relative researchers have focussed on some basic issues such as initiation limit and process, stabilization morphology and oscillation problems, etc. However, incoming boundarylayer effect would doubtless influence these basic issues and attention should be paid to them because this effect is inevitable in supersonic and hypersonic aircraft. In the ODWE concept, an ODW is often associated with a wedge hanging in the air which induces an oblique shock wave that ignites the premixed gas. The ODW can be stabilized on the wedge if the speed of incoming flow is high enough. Like a shock wave, there exists a maximum wedge angle beyond which the ODW will be a detached one. However, theoretically speaking, there is also a minimum wedge angle which is referred to as the Chapman-Jouguet (CJ) angle for a stabilized ODW [18]. It has been found that the standing morphology of an ODW can be smooth or abrupt [19– 21]. For the former, there is no transverse wave between the induction shock and the detonation. For the latter, a transverse wave exists. For a wedge hanging in the air, it will endure huge thermal load (especially near the tip of the wedge) at the same time of supporting an ODW. If the wedge is mounted on the floor to become a ramp, the thermal load near the tip will be significantly relieved. However, the ramp will also bring in influence of an incoming boundary layer. It can be reasonably deduced that the standing morphology of an ODW may be different when there is a boundary layer in the incoming flow because of possible interactions between the ODW and the boundary layer. Such an influence will be numerically studied in the following paragraphs.

# 2 Physical model and numerical method

The two-dimensional computational domain is shown in Figure 1. The incoming flow is H2/air premixed gas and is at a Mach number of 3.0, static temperature of 850 K, static pressure of 10 kPa, and an equivalence ratio of 0.4. The incoming flow encounters a compression ramp and the oblique detonation wave is produced. The ramp surface has a length of 200 mm and the ramp angle is 24 degrees.

The basic governing equations are two-dimensional Navier-Stokes equations which are given as

$$\frac{\partial \mathbf{Q}}{\partial t} + \frac{\partial (\mathbf{E} - \mathbf{E_v})}{\partial x} + \frac{\partial (\mathbf{F} - \mathbf{F_v})}{\partial y} = \mathbf{H}$$

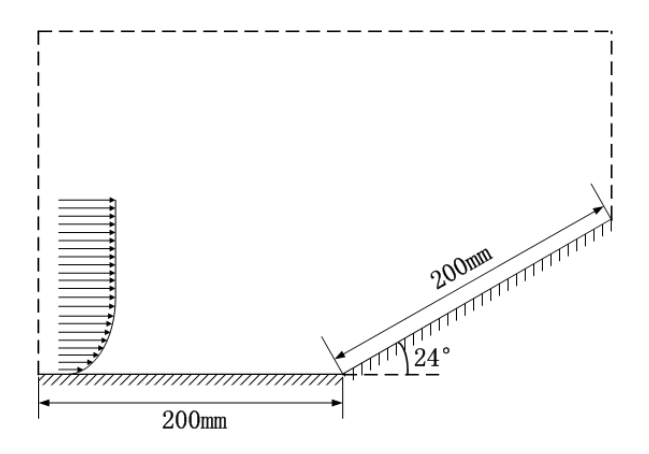


Figure 1: Physical model

where Q, E, F, G are the advection vectors given by

$$\mathbf{Q} = \begin{bmatrix} \rho \\ \rho u \\ \rho v \\ \rho e \\ \rho Y_i \end{bmatrix} \quad \mathbf{E} = \begin{bmatrix} \rho u \\ \rho u u + p \\ \rho u v \\ u(\rho e + p) \\ \rho u Y_i \end{bmatrix} \quad \mathbf{F} = \begin{bmatrix} \rho v \\ \rho v v + p \\ \rho u v \\ v(\rho e + p) \\ \rho v Y_i \end{bmatrix}$$

Ev, Fv, Gv, are the diffusion vectors given by

$$\mathbf{E}_{\mathbf{v}} = \begin{bmatrix} 0 \\ \tau_{xx} \\ \tau_{xy} \\ u\tau_{xx} + v\tau_{xy} - q_x \\ \rho D_i \partial Y_i / \partial x \end{bmatrix} \mathbf{F}_{\mathbf{v}} = \begin{bmatrix} 0 \\ \tau_{yx} \\ \tau_{yy} \\ u\tau_{xy} + v\tau_{yy} - q_y \\ \rho D_i \partial Y_i / \partial y \end{bmatrix}$$

$$\mathbf{H} = \begin{bmatrix} 0 \\ 0 \\ 0 \\ 0 \\ 0 \\ 0 \end{bmatrix}$$

In the above flux vectors,  $\rho$  is the density of the fluid. u and v are the components of velocity in the x, y directions, respectively. p is the pressure, and e is the inner energy of the fluid particle.  $q_x$  and  $q_y$  are the heat flux in the x, y directions, respectively.  $Y_i$  is the mass fraction of each species i.  $D_i$  is the diffusion coefficient of species i.  $\omega_i$  is the net rate of production of species i by chemical reaction which will be described later.  $\tau_{xx}$ ,  $\tau_{xy}$ ,  $\tau_{yx}$ ,  $\tau_{yy}$  are the stress tensors given by

$$\tau_{xx} = \lambda \left( \frac{\partial u}{\partial x} + \frac{\partial v}{\partial y} \right) + 2\mu \frac{\partial u}{\partial x}$$

$$\tau_{yy} = \lambda \left( \frac{\partial u}{\partial x} + \frac{\partial v}{\partial y} \right) + 2\mu \frac{\partial v}{\partial y}$$

$$\tau_{xy} = \tau_{yx} = \mu \left( \frac{\partial v}{\partial x} + \frac{\partial u}{\partial y} \right)$$

where  $\mu$  is the dynamic viscosity coefficient and  $\lambda$  is the Stokes viscosity coefficient which equals  $-\frac{2}{3}\mu$ .

As we know, in order to describe the turbulence characteristics of the fluid, variables in the Navier-Stokes equations should be decomposed into mean and fluctuating components. For example, the velocity component u and v can be decomposed as  $u = \bar{u} + u'$  and  $v = \bar{v} + v'$ , respectively, where  $\bar{u}$  and  $\bar{v}$  are the mean components, and u' and v' are the fluctuating components. After decomposing, the final form of the Navier-Stokes equations is the same as the original except that new turbulence terms,  $-\rho \overline{u'^2}$ ,  $-\rho \overline{v'^2}$  and  $-\rho \overline{u'v'}$ , called Reynolds stresses, are introduced into the equations. The final form of the equations are called Reynolds averaged Navier-Stokes (RANS) equations. In order to model Reynolds stresses to close the RANS equations, different turbulence models are proposed in past decades. In this paper, the Spalart-Allmaras (SA) turbulence model [22] is employed in the numerical code because this model is proved to behave well in the simulation of flow field involving boundary layer separation induced by the shock wave (see the next section). This model is based on the Boussinesq hypothesis which relates the Reynolds stresses to the mean velocity gradients:

$$\begin{split} &-\rho\overline{u'v'} = \mu_t \left(\frac{\partial \bar{u}}{\partial y} + \frac{\partial \bar{v}}{\partial x}\right) \\ &-\rho\overline{u'^2} = 2\mu_t \frac{\partial \bar{u}}{\partial x} - \frac{2}{3} \left(\rho k + \mu_t \left(\frac{\partial \bar{u}}{\partial x} + \frac{\partial \bar{v}}{\partial y}\right)\right) \\ &-\rho\overline{v'^2} = 2\mu_t \frac{\partial \bar{v}}{\partial y} - \frac{2}{3} \left(\rho k + \mu_t \left(\frac{\partial \bar{u}}{\partial x} + \frac{\partial \bar{v}}{\partial y}\right)\right) \end{split}$$

where  $\mu_t$  is the turbulent viscosity and k is the turbulent kinetic energy which equals  $\frac{1}{2}\left(\overline{u'^2}+\overline{v'^2}\right)$ . The aim of the turbulence model is to solve the turbulent viscosity. The model equation of the SA turbulence model is given as:

$$\begin{split} &\frac{\partial}{\partial t} \left( \rho \tilde{v} \right) + \frac{\partial}{\partial x} \left( \rho \tilde{v} u \right) + \frac{\partial}{\partial y} \left( \rho \tilde{v} v \right) = \\ &G_v + \frac{1}{\sigma_{\tilde{v}}} \left\{ \frac{\partial}{\partial x} \left[ \left( \mu + \rho \tilde{v} \right) \frac{\partial \tilde{v}}{\partial x} \right] + \frac{\partial}{\partial y} \left[ \left( \mu + \rho \tilde{v} \right) \frac{\partial \tilde{v}}{\partial y} \right] \right. \\ &\left. + C_b \rho \left[ \left( \frac{\partial \tilde{v}}{\partial x} \right)^2 + \left( \frac{\partial \tilde{v}}{\partial y} \right)^2 \right] \right\} - Y_v \end{split}$$

where the transported variable,  $\tilde{v}$ , can be used to compute the turbulent viscosity. That is,  $\mu_t = \rho \tilde{v} \frac{\left(\frac{\tilde{v}}{v}\right)^3 + C_v^3}{\left(\frac{\tilde{v}}{v}\right)^3 + C_v^3}$ , where v is the molecular kinematic viscosity and  $C_v$  is a constant.  $G_v$  and  $Y_v$  is the production and destruction of turbulent viscosity, respectively. Modeling of both  $G_v$  and  $Y_v$  can be found in reference [22], and details will not be given here.

In the Navier-Stokes equations,  $\omega_i$  is the net rate of production of species i by chemical reaction. It can be ex-

pressed as:

$$\omega_i \simeq M_i k_f \prod_{i=1}^N c_i^{\nu_i'}$$

where  $M_i$  is the molecular weight of species i,  $k_f$  is the reaction rate constant,  $c_i$  is the molar concentration of species i, and  $v_i'$  is the reaction coefficient of a certain chemical reaction. It is clear that the reaction rate constant  $k_f$  is the core factor to resolve for chemical reactions. Since the subject of this paper is the interaction between the oblique detonation wave and the boundary layer, the influence of turbluence on chemistry is a relevant issue, especially in the separation region where turbluent combustion may exist. Popular processing methods of turbulence-chemistry interaction in recent years include flamelet model and probability density function (PDF) model [23], etc. However, these turbulence-chemistry treatments have not vet been used in detonation simulations, for which turbulencechemistry interaction is neglected and only Arrhenius finite-rate chemistry is taken into account. Thus, relevant experiences are absent and in this paper, we still consider Arrhenius finite-rate chemistry only to compute  $k_f$ , that is

$$k_f = AT^b \exp\{-E_\alpha/RT\}$$

where A is the pre-exponential factor,  $E_{\alpha}$  is the activation energy for the reaction, R is the universal gas constant, and T is the temperature. For one-step global reaction of hydrogen/air mixture,  $H_2 + \frac{1}{2}O_2 = H_2O$ , these parameters are given as  $A = 9.87 \times 10^8$ , b = 0,  $E_{\alpha} = 3.1 \times 10^7$  j/kg· mol.

Different wall conditions are imposed to the lower boundary of the computational domain to realize control on the separation scales. These conditions include a noslip, adiabatic wall condition, a no-slip, cold wall condition and a slip wall condition.

The inviscid flux vector of the governing equations are processed using Roe's flux-difference splitting scheme [24]. The convection terms are discretized by second-order upwind scheme with the flux-limiter which can eliminate oscillation around discontinuities such as shock waves. The diffusion terms are discretized by central-difference scheme which is also second-order accurate. As for the time stepping method, a second-order implicit scheme which is known as 'dual-time stepping' is employed to ensure the temporal accuracy. Besides, perfect-gas properties are employed and real-gas effects are not considered in this paper.

Grid generation for current simulation is another important issue because both the near-wall flow and the ODW require sufficient grid resolution. For the former, grids in the boundary layer are generated so that the wall-adjacent grid is located in the viscosity-affected layer, i.e.,

18 — Y. Liu et al. DE GRUYTER OPEN

on the order of  $y^+ = 1$ . For the latter, adaptive mesh refinement is applied to clearly capture the discontinuities of the flow field. Across the ODW, the maximum refinement level is 4 and corresponding grid scale reaches as small as 0.05  $\times$  0.05 mm<sup>2</sup>.

## 3 Code validation

In order to test the numerical method's reliability in current simulation, both the boundary layer separation and the ODW should be included in the experiment of validation. Unfortunately, there are no such experiments so far as we know. However, we can compromise to choose experiments of SWBLI to conduct code validation.

The experiment conducted by Dolling and Murphy [25] on the SWBLI problem in 1982 is chosen to conduct code validation. In this experiment, the incoming flow is at a Mach number of 2.9, a total pressure of 680 kPa and a stagnation temperature of 265 K. The incoming boundary layer is 2.2-cm thick, giving a Reynolds number of  $7.8 \times 10^5$  based on its thickness. The ramp angle is 24 degree and both the length and the width of the ramp surface are 15 cm. The flow field has been proved to present two-dimensional features very well.

Figure 2 and Figure 3 respectively gives comparison of shadowgraphs and wall-pressure ( $P_w$ ) distributions between the experiment and the numerical simulation. Results show good agreements, which prove that the numerical method is proper for simulating flow field involving large-scale separation due to shock wave-boundary layer interactions.

#### 4 Results and discussion

First, a no-slip, adiabatic wall condition is employed to the lower boundary of the computational domain and thus a boundary layer is developed from the inlet. Without considering chemical reactions, a typical flow field of shock wave-boundary layer interactions is presented in Figure 4 as a velocity contour.

It can be seen that under current condition, the 'cold' flow field which does not contain reactions involves boundary layer separation due to considerable shock wave strength. The sudden jump of pressure in the inviscid case is now replaced by a milder rise, as is illustrated in Figure 5. It is also shown that the separation region can be reduced when a non-adiabatic, cold wall condition of  $\frac{T_w}{T_0}$ , where  $T_w$  is the wall temperature and  $T_0$  the stagnation

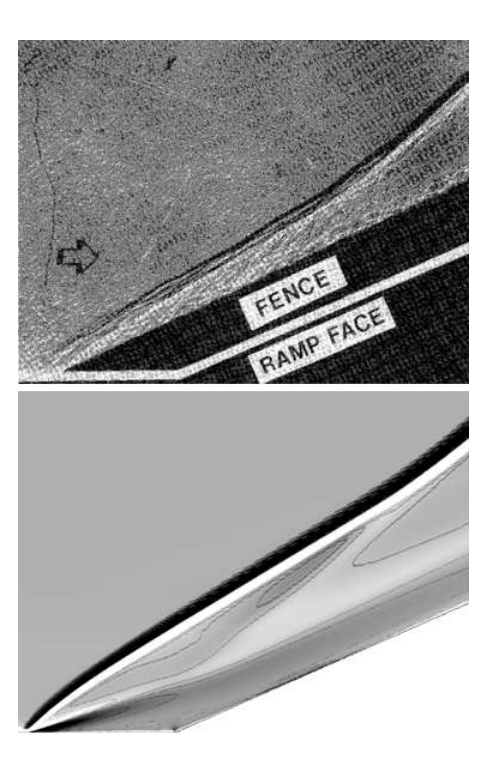
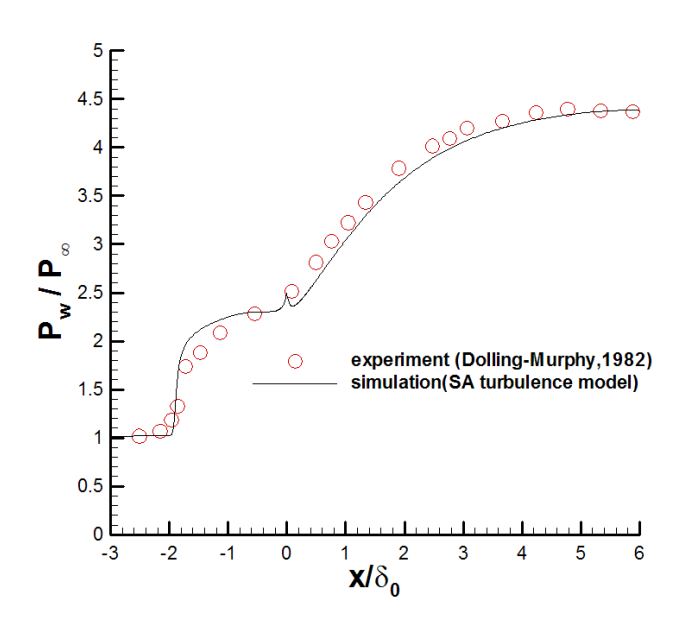


Figure 2: Comparison between the experimental [25] (upper) and numerical (lower) shadowgraphs



**Figure 3:** Comparison between the experimental and numerical wall-pressure distributions ( $P_{\infty}$  indicating the freestream static pressure, and the same for following figures)

temperature of the incoming flow, is applied. Such a tendency can be attributed to two reasons. First, the cold wall makes the density level in the boundary layer raised, and hence a larger skin-friction coefficient which provides more resistance to the adverse pressure gradients. Second, the contraction of the separation region is also a conse-

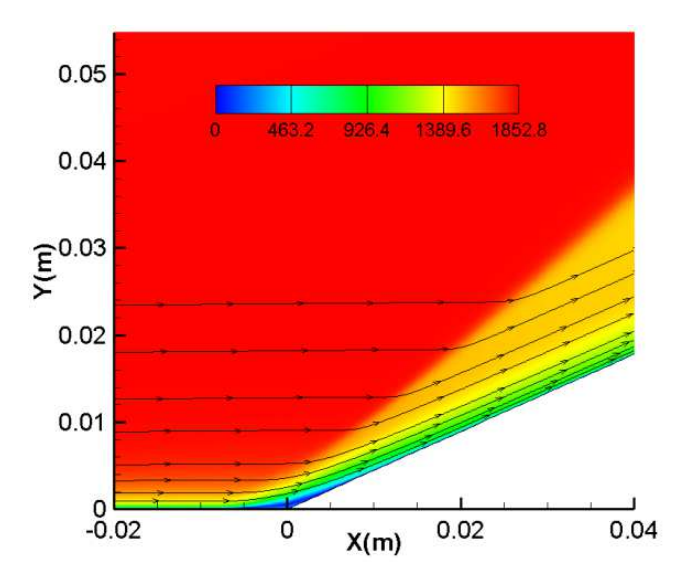


Figure 4: Velocity magnitude (m/s) and streamlines of cold flow field with no-slip, adiabatic wall condition

quence of the thinning of the boundary-layer subsonic part because the Mach number in the inner part of the boundary layer is greater due to lower sound speed (i.e., lower temperature). Thus, it can be reasonably predicted that this trend also holds in cases where there exist reactions behind the shock waves, which will be confirmed later.

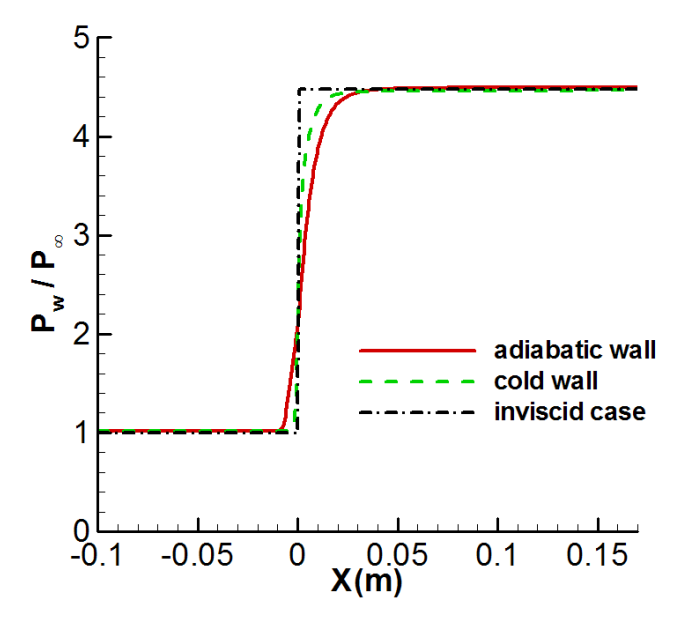


Figure 5: Wall-pressure distribution of cold flow field with different wall conditions

When solving the 'hot' flow field where there are chemical reactions (residual errors reach the order of  $10^{-9}$ , indicating that the computation has been converged), an

ODW is formed which induces even larger scales of separation region because of the stronger detonation strength (see Figure 6). Realizing the incoming boundary layer in hot flow field may be different from that in the cold since there may exist reactions within the boundary layer because of high temperature in it, certain numerical treatments are performed to suppress boundary layer reactions (except in the separation region) to eliminate such a difference, although it is not so physical to do so. This treatment is simply turning off the reaction unless the pressure reaches more than 1.1 times the freestream pressure. It can be seen that the boundary layer separates at about x = -0.082 m where separation shock emanates from, and a series of compression waves follow thereafter due to combustion induced by the separation shock. It seems that the separation streamline now acts as an aerodynamic ramp whose angle is smaller than that of the real physical ramp. Since this aerodynamic ramp is sufficiently long because the separation region is large, these compression waves gradually strengthen the shock and the shock-wave angle is continuously risen up. Finally, the ODW is standing at a smooth manner, for which there is no typical transverse wave structure between the induction shock (i.e., the separation shock) and the detonation wave. However, when the same cold wall condition as that in the cold flow field is imposed, as is shown in Figure 7, the separation region is considerably contracted, and the aerodynamic ramp is therefore shortened. Thus, the real physical ramp now has opportunity to provide another stronger compression effect. As a result, compression waves focus together, giving a significant strengthening effect, at the point where the wave angle has a sudden change. Instead of presenting a smooth pattern, the ODW now becomes an abrupt one for which a transverse wave exists in order to match the pressure of the upper part and the lower part of the main flow. This trend of contraction of separation region for cold wall condition is similar to that in SBLI problem, as predicted sooner.

In order to further investigate the influence of incoming boundary layer, a slip wall condition is applied. That is to say, there is no boundary layer in the incoming flow, and another different structure of ODW is obtained, as is shown in Figure 8. Without boundary layer, the ODW under current condition is detached, presenting a bow shape just ahead of the ramp corner. That is to say, the ramp angle of 24 degree actually exceeds the maximum standing angle of the ODW under current condition. Thus, the standing morphology of the ODW is significantly influenced by its interaction with the boundary layer. Figure 9 shows overlaid wall-pressure distributions of all cases for easy comparison. It can be seen that the peak pressure of slip-wall case

20 — Y. Liu et al. DE GRUYTER OPEN

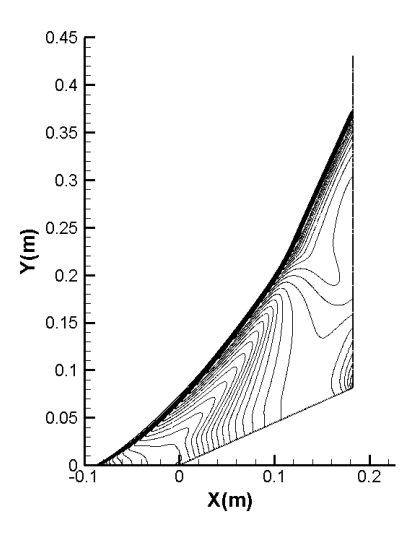


Figure 6: Pressure contour of hot flow field with no-slip, adiabatic wall condition (40 levels from 10 kPa to 81.1 kPa)

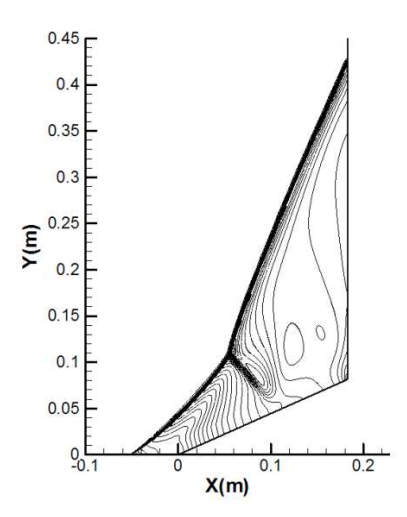


Figure 7: Pressure contour of hot flow field with no-slip, cold wall condition (40 levels from 10 kPa to 95.5 kPa)

is over 10 times the freestream pressure because of bowshaped normal detonation wave just ahead of the ramp origin. However, for adiabatic and cold-wall cases, peak pressures are much lower than slip-wall case, although the incoming-flow conditions are the same for all the three cases. This is the typical effect of the boundary-layer separation. Despite of the difference of peak pressures, the final wall-pressure levels of the three cases have the same trends although for the no-slip, adiabatic wall condition, longer distance will be required for the wall pressure to reach the slip-wall level because of the larger separationto-reattachment region.

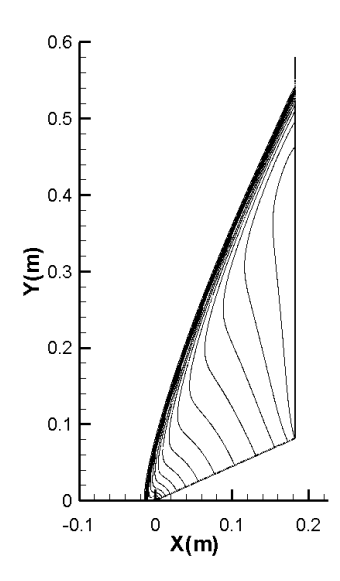


Figure 8: Pressure contour of hot flow field with slip wall condition (40 levels from 10 kPa to 110.7 kPa)

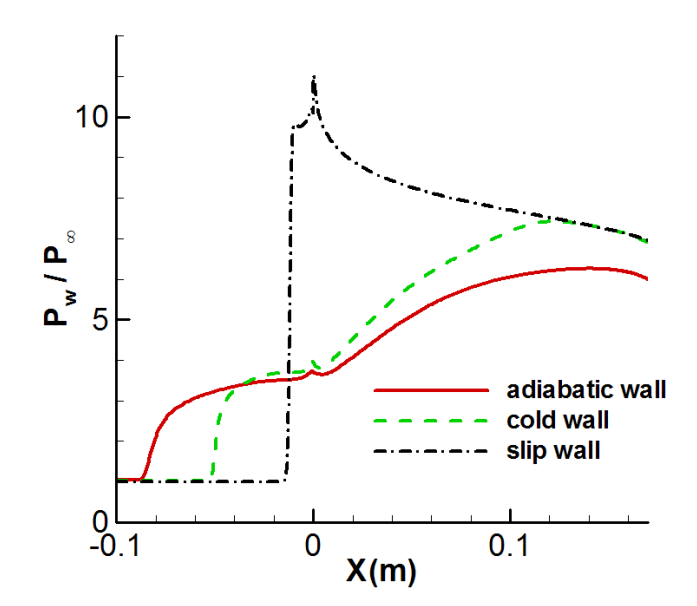


Figure 9: Wall-pressure distributions of different wall conditions

# **5 Conclusions**

In this paper, the influence of an incoming boundary layer to the standing morphology of an ODW induced by a ramp in supersonic premixed flows is numerically investigated by solving two-dimensional coupled reacting Reynolds-Averaged Navier-Stokes equations with Spalart-Allmaras turbulence model. With everything else the same, different wall conditions are imposed to control the boundary-layer separation scales. Results show that under no-slip, adiabatic wall condition, the separation scales are larger than that under no-slip, cold wall condition. For the former, the

standing morphology of the ODW is smooth, however, for the latter, it is abrupt. When a slip-wall condition is imposed, there is no boundary layer in the incoming flow, and the ODW stands in a detached manner, presenting a bow shape just ahead of the ramp origin. Although the study in this paper is based on simple one-step Arrehnius reaction, and turbulence-chemistry-interaction treatment is not considered, the results still have important implications for detonation-viscosity interactions, which have rarely been investigated before, due to traditional inviscid Euler equations employed in detonation simulations.

**Acknowledgement:** This work is supported by the National Natural Science Foundation of China under Grant Nos. 91016028 and 91216121.

### References

- [1] F. W. Spaid, J. L. Frishett, AIAA J. 10, 915 (1972)
- [2] G. S. Settles, S. M. Bogdonoff, I. E. Vas, AIAA J. 14, 50 (1976)
- [3] G. S. Settles, T. J. Fitzpatrick, S. M. Bogdonoff, AIAA J. 17, 579 (1979)
- [4] J. Green, Prog. Aerospace Sci. 11, 235 (1970)
- [5] E.E. Zhukoski, AIAA J. 5, 1746 (1967)
- [6] R.H. Korkegi, AIAA J. 13, 534 (1975)

- [7] M. S. Holden, AIAA 10th Aerospace Sciences Meeting, No.72-74, January 17-19, 1972, San Diego, California, USA
- [8] K. J. Plotkin, AIAA J. 13, 1036-1040 (1975)
- [9] B. Ganapathisubramani, N. T. Clemens, D. S. Dolling, J. Flui. Mech. 585, 369- (2007)
- [10] J. Fay, Phys. Fluids 2, 283 (1959)
- [11] E. K. Dabora, J. A. Nicholls, R. B. Morrison, Proc. Combust. Inst. 10, 817 (1965)
- [12] S. B. Murray, Ph.D. thesis, McGill University (Montreal, Canada, 1984)
- [13] W. P. Sommers, R. B. Morrison, Phys. Fluids 5, 241 (1962)
- [14] S. B. Murray, J. H. Lee, Prog. Astronaut. Areonaut. 106, 329 (1986)
- [15] C. Li, K. Kailasanath, E. S. Oran, 31st Aerospace Sciences Meeting and Exhibit, No.93-0450, January 11-14, 1993, Reno, NV, USA
- [16] J. Y. Choi, I. S. Jeung, Y. Yoon, Proc. Combust. Inst. 2181 (1998)
- [17] F.Giovanni, Ph.D. thesis, University of Toronto (Toronto, Canada, 2003)
- [18] D. T. Pratt, J. W. Humphrey, D. E. Glenn, J. Propulsion 7, 837 (1991)
- [19] L. Figueira Da Silva, B. Deshaies, Combust.Flame 121, 152 (2000)
- [20] A. F. Wang, W. Zhao, Z. L. Jiang, Acta Mech. 27, 611 (2011)
- [21] H. H. Teng, Z. L. Jiang, J. Fluid Mech. 713, 659 2012)
- [22] P. R. Spalart, S. R. Allmaras, AIAA J. 94 (1992)
- [23] N. Peters, Turbulent combustion, 3rd edition (Cambridge university press, Cambridge, 2000)
- [24] P. L. Roe, Annual Review of Fluid Mechanics, 18, 337 (1986)
- [25] D. S. Dolling, M. T. Murphy, AIAA J. 21, 1628 (1983)